Net Emission Coefficient and Radiation Transfer Characteristics of Thermal Plasma Generated in Nitrogen-PTFE Vapor Mixture

Jianying Zhong, Fei Yang, Wen Wang, Duanlei Yuan and Jiu Dun Yan

***Abstract*—The radiation characteristics of thermal plasma columns filled with N_2-PTFE vapour mixture has been studied for the first time. The net emission coefficient is first calculated for typical mixture concentrations. The Discrete Ordinate Method (DOM), which has proven to be an approximate method of reasonable accuracy for radiation transfer in thermal plasmas, is then used to characterise the emission and absorption behaviour of cylindrical plasma columns with typical temperature distributions. Results show that the radiative power loss per unit volume at the column centre is not always proportional to the local gas pressure. The DOM12-9 configuration, i.e. considering 24 directions in the r-plane of the calculation point and 18 directions crossing the r-plane, produces remarkably accurate results. It is likely to recover the accurate emission and absorption profile by scaling the output from the DOM5-3 configuration with a scaling factor between 0.7 and 0.8. Furthermore, the DOM5-3 configuration accurately locates the absorption layer at the edge of the plasma column. Maximum absorption takes place at a radial location whose distance to the inner radius of the absorption layer is 30% of the layer thickness despite of the very different radial temperature profiles. Under the conditions studied 35-60% of the radiation from the central part of the column is absorbed in the surrounding cooler gas.**

***Index Terms*—Radiation transfer, switching arc, N_2-PTFE mixture, Net emission coefficient, Discrete Ordinate Method**

I. Introduction

Nitrogen as an environmentally friendly gas has been tried in recent years as the working medium in switching equipment [1]-[4] to replace SF_6 that is an excellent insulating and arc quenching gas but also a strong greenhouse gas (Global Warning Potential: GWP = 23,500) with a life time of 3,200 years in the atmosphere. The arc in such equipment burns in the mixture of N_2 and Polytetrafluoroethylene (PTFE) vapour, with the latter being generated by nozzle ablation [5]. Radiation transfer plays a vital role in the energy balance of thermal plasmas. It is also responsible for polymer nozzle ablation in high voltage self-blast circuit breakers [6]. To facilitate theoretical studies on the application of N_2 in environmentally friendly circuit breakers, especially on computational fluid dynamics (CFD) modelling of the arcing process, thermodynamic and transport properties as well as a model for radiation transfer in the N_2 and PTFE vapour mixture are required. While there is limited published work on the thermodynamic properties and transport coefficients [7], no work has been reported on the radiation emission characteristics of the gas mixture, such as the net emission coefficient (NEC) or the calculation of the net radiative energy loss from an arc column.

Radiation emission and absorption coexist in the arcing gas but it is the hottest arc core that emits more radiation than it absorbs. As a result, there is a net flux of radiation leaving the arc core which is subsequently absorbed in part in the relatively colder region that surrounds this arc core. The percentage of the radiative flux that is absorbed depends on the type of gas and the distribution of temperature, pressure and gas composition in the gas domain. Radiation that penetrates the arc surrounding gas and reaches the polymer wall of a circuit breaker nozzle causes strong nozzle ablation at high current. It is the hot vapour generated at the nozzle surface that creates a high pressure zone in the main nozzle that subsequently drives the hot vapour into the heating chamber to form a high pressure gas reservoir. The stored high pressure gas flows towards the main nozzle when the arc current approaches its zero point and forms a high speed flow environment for arc quenching [5]. Thus, radiation transfer plays a central role in shaping the interruption performance of a self-blast circuit breaker.

Radiation transfer is however an extremely complicated phenomenon. Accurate solution of the radiation transfer equation (RTE) is prohibitively expensive in terms of computation time for a complex engineering system such as a high voltage circuit breaker. Firstly, integration over three dimensional space needs to be carried out to account for the emission contribution from all hotter gas towards the point of calculation. Secondly, integration over all wavelengths of the spectra has to be performed to account for the total emission.

This paragraph of the first footnote will contain the date on which you submitted your paper for review. It will also contain support information, including sponsor and financial support acknowledgment. For example, "This work was supported in part by the U.S. Department of Commerce under Grant BS123456."

Jianying Zhong and Duanlei Yuan are with Pinggao Group Co. Ltd., Pingdingshan City, Henan, China 467001.

Fei Yang and Wen Wang are with the Department of Electrical Engineering and Electronics, the University of Liverpool, Liverpool, L69 3GJ, UK.

Jiu Dun (Joseph) Yan is with the Department of Electrical Engineering and Electronics, the University of Liverpool, Liverpool, L69 3GJ, UK. (e-mail: yaneee@liverpool.ac.uk).

Lastly, the absorption and emission strengths (coefficients) at each wavelength must be calculated based on the local temperature, pressure, gas composition and information on the energy levels. It is thus necessary to have a simplified method of radiation transfer calculation that is acceptable in computation time and also in accuracy for design modelling purposes.

There are a number of approximate methods for radiation transfer calculation. The P1 approximation was probably the earliest method to approximate radiation transfer in thermal plasmas. It was proposed by Jeans [8] first in 1917 and described in further details by Kourganoff [9] in 1952. A simple partial differential equation (PDE) is used to approximate the radiation transfer process. This method has reasonable accuracy for gases with near-isotropic radiation characteristics because it involves averaging the radiation absorption coefficients of a gas over different wavelengths [10]. The Partial Characteristics Method (PCM) was developed by Sevast'yanenko [11] which uses two characteristic parameters, designated normally by Som and ΔSim, to account for the cumulative emission from a source of emission to a target point in straight line and for the net effect of radiation absorption at a point. The advantage is that these two values can be pre-calculated and tabulated for a known gas with uniform pressure to reduce computational effort. Its application is however still very limited since the pressure in the arcing chamber of a circuit breaker varies significantly due to magnetic pinch and fluid dynamics and this spatial pressure variation cannot be fully considered in the calculation of the two parameters. This method is thus not recommended for practical switching arc modelling.

The Discrete Ordinate method (DOM) [12] is an improved approximate method and has been used in arc modelling in recent years [13], [14]. With this method, one dimensional radiation transfer is performed along chosen discrete directions and the results are summed with a weighting factor to account for the 4π solid angle. Theoretically the pressure variation in the arcing gas can be accounted for. Its accuracy depends on the number of directions (discrete ordinates) used [13]. There is still a lack of definitive conclusion on its accuracy as a function of the number of integration directions under different arcing conditions. The primary objective of the present work is thus to gain in-depth understanding of its important behavioural features under conditions close to real applications.

The concept of net emission coefficient (NEC) was introduced by Lowke in 1974 [15] for an infinitely long, isothermal and cylindrical plasma column. It has since been used widely in the modelling of thermal plasmas [5], [16], [17] with much success. However, its accuracy in representing the radiative energy loss from a thermal plasma column depends on the choice of an effective emission radius since in reality an arc column has limited length and is seldom isothermal. Furthermore, there can be large pressure variations across the column radius such as in high voltage self-blast circuit breakers [18]. Because of the simplicity to obtain solution, it is still used in arc modelling involving full scale circuit breakers.

In the present work, the NEC of N_2-PTFE vapour mixtures will be calculated in Sections 2 and 3 at different pressures and PTFE concentration. This is followed by a study in Section 4 of the radiative characteristics of cylindrical arc plasma columns with two typical radial temperature distributions. Knowledge of these features is vital to the development of approximate radiation transfer models. Conclusions are drawn in Section 5.

TABLE I
Chemical species considered in the calculation of plasma composition.

Species in Set z^*	Constituting chemical basis ($c_{j,i}$)			
	e-	N+	CN	C_2F_2
N_2	2	2	0	0
C_2	-2	-2	2	0
F_2	2	2	-2	1
N	1	1	0	0
N_2+	-1	1	0	0
N_3+	-2	1	0	0
F	1	1	-1	0.5
F+	0	1	-1	0.5
F_2+	-1	1	-1	0.5
F_3+	-2	1	-1	0.5
F_4+	-3	1	-1	0.5
C	-1	-1	1	0
C+	-2	-1	1	0
C_2+	-3	-1	1	0
C_3+	-4	-1	1	0
C_2F_4	2	2	-2	2
CF_2	1	1	-1	1
CF_3	2	2	-2	1.5
C_2F_3N	2	2	-1	1.5
CF_4	3	3	-3	2
C_2N_2	0	0	2	0
FN	2	2	-1	0.5

II. Absorption Coefficient and Net Emission Coefficient

A. Calculation of plasma composition

The radiation emission characteristics of gas depends on the species and their concentrations. A robust and efficient method, originally proposed by Godin and Trepanier [19], is used to calculate the composition of the gas or gas mixture in Local Thermal Equilibrium (LTE) and Local Chemical Equilibrium (LCE) states. In the present study a total of 26 species are taken into account. Carbon radicals with more than three atoms are not considered. Following Godin and Trepanier [19], a set of chemical basis are defined. The number of chemical basis must be equal to the number of elements in the mixture plus the charge which is regarded as an independent chemical basis. Thus the species are divided into two groups, with the first group (Set z) consisting of the M chemical basis (M=4) and the second group (Set z^*) containing the remaining L-M species (L=26). The chemical species considered can be found in Table I.

The relationship between the reactants and products in a chemical reaction including ionisation and recombination is governed by the mass action law. At equilibrium all chemical species in Set z* are related to the 4 chemical basis in Set z by

$$n_{z_j^*} = Q_{z_j^*} \prod_{i=1}^{M} \left(\frac{n_{z_i}}{Q_{z_i}}\right)^{c_{j,i}} \quad (1)$$

where n is number density, Q the partition function and subscripts z_j^* and z_i represent, respectively, species j in Set z* and species i in Set z. $c_{j,i}$ is a coefficient relating to chemical basis i when species j is composed using the chemical basis. The values for $c_{j,i}$ are also given in Table I for each species in Set z*.

Equation (1) in fact represents 22 independent equations (Table II). In addition, another 4 equations can be constructed based on the fixed ratio of the total number of atomic nuclei (the fixed ratio of C:F contained in PTFE and ratio of F:N between PTFE and N_2), charge neutrality and Dalton's law. These 4 equations are referred to as the base equations below for convenience. A total of 26 equations are therefore obtained. Logarithm is taken on both sides of the 22 equations in the form of Equation (1) to obtain 22 linear equations with the logarithm of number density as the variables. The linear equations are then substituted in the base equations to reduce the total number of unknowns to only 4, i.e. the number density of the 4 chemical basis. This gives a smaller size of the Jacob matrix in the Newton-Raphson method, greatly promoting the convergence speed of the solution process.

TABLE II
List of chemical reactions in the calculation

No.	Chemical reaction	No.	Chemical reaction
1	$N_2 \leftrightarrow N + N$	12	$F \leftrightarrow F^+ + e^-$
2	$N \leftrightarrow N^+ + e^-$	13	$F^+ \leftrightarrow F^{2+} + e^-$
3	$N^+ \leftrightarrow N^{2+} + e^-$	14	$F^{2+} \leftrightarrow F^{3+} + e^-$
4	$N^{2+} \leftrightarrow N^{3+} + e^-$	15	$F^{3+} \leftrightarrow F^{4+} + e^-$
5	$C_2F_4 \leftrightarrow C_2F_2 + F_2$	16	$C \leftrightarrow C^+ + e^-$
6	$C_2F_2 \leftrightarrow C_2 + F_2$	17	$C^+ \leftrightarrow C^{2+} + e^-$
7	$F_2 \leftrightarrow F + F$	18	$C^{2+} \leftrightarrow C^{3+} + e^-$
8	$C_2 \leftrightarrow C + C$	19	$C^{3+} \leftrightarrow C^{4+} + e^-$
9	$C_2F_3N \leftrightarrow CF_3 + CN$	20	$CF_2 \leftrightarrow C + F + F$
10	$CN \leftrightarrow C + N$	21	$CF_4 \leftrightarrow CF_3 + N$
11	$CF_3 \leftrightarrow CF_2 + F$	22	$FN \leftrightarrow F + N$

TABLE III
Sources for basic atomic data used to calculate the partition functions

Atomic data	Species	Source of information
Energy levels (electronic, vibration and rotation)	atoms, ions and molecules	ASD of NIST [20], Kurucz [21]
Statistical weight	All discrete energy levels	ASD of NIST [20], Kurucz [21]
Reaction energy	For all chemical reactions	Table 3
Reference energy		Table 4
Symmetry factor	For rotational partition function	2 for homonuclear molecules and 1 for heteronuclear molecules
Spectroscopic parameters	For the calculation of vibrational and rotational energy levels of molecules.	JANAF [22], Wiese [23]

B. Calculation of partition functions

Calculation of the partition functions of the gas mixture requires knowledge of the atomic parameters as described in Table III. The partition function of monatomic species is calculated by summation over all energy levels below the ionization limit while the summation for high energy levels is replaced by integration. The partition function of molecules is a product of Q_{ele}, Q_{vib} and Q_{rot}, representing, respectively, the electronic, vibrational and rotational partition functions. The reference energy for each species is given in Table IV.

C. Radiation emission and absorption

Radiation from a high temperature gas consists of line (bound-bound) and continuum emissions. The emission of line spectra is caused by transitions of excited neutral particles (atoms and molecules) or ions from higher energy levels to lower ones. When an electron is captured by an atom or ion into its orbit, the recombination process leads to the emission of free-bound radiation. In general, this mechanism can apply to all possible energy levels of a molecule, atom or ion. Therefore, all species can emit continuum spectra resulting from free-bound radiation. Bremsstrahlung (free-free transition) is another process that produces continuum radiation. A free electron may lose part of its kinetic energy due to interaction with other charged particles through Coulomb field. Radiation in this situation is converted from the lost kinetic energy of the charged particles. Recombination and Bremsstrahlung contribute most towards the continuum radiation. The radiation spectrum also contains molecular bands which are a result of extinction of the rotational and vibrational energy of molecules.

Equation (2) below describes the variation of monochromatic radiative intensity I_ν over a thickness L in a gas in the direction of propagation,

$$I_\nu = I_{\nu 0} \exp\left(-\int_0^L \kappa_\nu dx'\right) = I_{\nu 0} \exp(-\tau_\nu) \quad (2)$$

where κ_υ is the absorption coefficient (m^{-1}) at frequency ν a nd $I_{\nu 0}$ the initial intensity. The absorption coefficient is applica ble to line and continuum radiation.

1) Line emission, broadening and shifting

Due to the important influence of line overlapping on radiative transfer, all overlapped spectral lines are taken into account in the calculation of the absorption coefficient. The absorption coefficient for a spectral line i emitted from species *'a'* can be denoted as [24]

$$\kappa_{a,\nu}^{i}(T,P) = \pi r_0 c f_{mn}^{a,i} N_n^a(T,P) L^i(\nu,T,P) \quad (3)$$

where r_0 is the classical electron radius, $f_{mn}^{a,i}$ the absorption oscillator strength of spectral line i corresponding to an electronic transition from higher energy level m to lower energy level n of specie a. N_n^a represents the population density of

lower energy level n of specie a. L^i is the normalized line profile,

$$2\int_0^\infty L^i(\nu,T,p)\,d\nu = 1 \tag{4}$$

where ν is the frequency. L^i is assumed to be of dispersion type or have Lorentz profile [24]. It can be expressed as

$$L^i(\nu,T,p) = \frac{1}{\pi\omega^i(T,P)(X^2+1)} \tag{5}$$

where $X = (\nu-\nu_c^i)/\omega^i(T,P)$, $\nu_c^i = \nu_0^i + d^i(T,P)$ and $\nu_0^i = \frac{E_m-E_n}{h}$. ν_c^i is the centre frequency of spectral line i and ω^i its half width. Due to perturbation on the energy states of atoms or ions, the frequency of peak absorption is slightly shifted from the ideal line centre which is at ν_0^i by a frequency interval of $d^i(T,P)$. The absorption coefficient for free-bound radiation from species a can be described by.

$$\kappa_\nu^{rec} = \sum_i \sigma_{i,\nu}^a N_i^a \tag{6}$$

where $\sigma_{i,\nu}^a$ is the photon absorption cross section at frequency ν by a particle at energy level i. N_i^a is the population density of specie a at E_i^a.

Radiation through transition between electronic energy levels often has a broadened line profile. The broadening of spectral lines can be caused by different mechanisms. When the population of charged particles dominates the total population of particles in a thermal plasma, the normal energy levels will be perturbed, which results in Stark broadening. This is true in our case when the temperature is above 20,000 K. Griem [2] has developed a theory for both atomic and ionic spectral lines.

TABLE IV
Reference energy (eV) for all species

Species	Reaction E
e^-	0
F_2	0
F	0.82 eV
F^+	18.242 eV
F^{2+}	53.214 eV
F^{3+}	115.922 eV
C_2F_2	-9.118 eV
CF_3	-10.657 eV
CF_4	-15.504 eV
N_2	0
N	4.88eV
N^+	19.42 eV
N^{2+}	49.025 eV
N^{3+}	96.451 eV
C^{4+}	151.226 eV
C_2F_4	-18.8 eV
CN	0.307 eV
C_2N_2	-5.314 eV
C_2	0
C	3.2eV
C^+	14.460 eV
C^{2+}	38.845 eV
C^{3+}	86.733 eV
F^{4+}	203.097 eV
CF_2	-5.81 eV
C_2F_3N	-15.211 eV
FN	2.083 eV

For ionic lines the half width and frequency shift are

$$\omega_{stark}^i = \mathrm{C(T,P)}\cdot\left[\sum_{J''}\frac{S(J'',J)}{2J+1}g_{Se}(X_{J''J}) + \sum_{J''}\frac{S(J'',J')}{2J'+1}g_{Se}(X_{J''J'})\right] \tag{7}$$

$$\mathrm{d}_{stark}^i = \mathrm{C(T,P)}\cdot\left[\sum_{J''}\frac{\Delta E_{J''J}}{|\Delta E_{J''J}|}\frac{S(J'',J)}{2J+1}g_{Sh}(X_{J''J}) - \sum_{J''}\frac{\Delta E_{J''J'}}{|\Delta E_{J''J'}|}\frac{S(J'',J')}{2J'+1}g_{Sh}(X_{J''J'})\right] \tag{8}$$

where J' and J are, respectively, the total angular momentum quantum numbers corresponding to energy levels m and n of spectral line i. $S(J'',J)$ and $S(J'',J')$ represent the line strength emitted as a result of transition to energy level n (J) and energy level m (J'). X are empirical functions given by Griem [2]. Function C is related to the population of free electrons:

$$\mathrm{C(T,P)} = 16\left(\frac{\pi}{3}\right)^{\frac{2}{3}} cR_\infty a_0^3 N_e\left(\frac{hcR_\infty}{kT}\right)^{1/2} \tag{9}$$

where R_∞ is the Rydberg constant, a_0 the Bohr radius and N_e the electron number density. The line strength can be calculated by

$$S(J',J) = 3(2J+1)\lambda R_\infty f_{J'J} \tag{10}$$

where $f_{J'J}$ is the atomic oscillator strength. The summation in Equations (7) and (8) is done over all possible transitions. Although the Stark broadening should be obtained by considering all transitions to and from the lower and upper energy levels, transitions between energy levels whose effective quantum numbers exceed 5 have negligible contribution towards the total broadening and can be neglected.

Resonance broadening can increase the half width of a spectral line when transition between the ground state and either the lower or upper energy level of the line is allowed. The resonance broadening of the half width of a spectral line is given by Liebermann and Lowke [24],

$$\omega_{Res}^i = \frac{3r_0c^2}{4\pi}\left[\frac{G_1}{G_K}\right]^{1/2}\frac{f_{K1}}{\nu_{Res}}N_1^a \tag{11}$$

where K refers to the lower or upper energy level that is allowed to transit to ground state. When K = 1, it refers to ground state. $G_K = (2S_K+1)(2L_K+1)$ and L is related to L-S coupling. S and L are, respectively, the spin angular momentum and orbital angular momentum in LS coupling. $\nu_{Res} = (E_K - E_1)/h$.

Van der Waals force exists among particles in thermal plasma. It is a much weaker force than chemical bond. However, it still perturbs the emitting particles. Equation (12) below describes the half width of a spectral line due to Van der Waals force

$$\omega_\nu^i = \frac{a_0^2}{2}\left[\frac{9\pi\alpha c}{4}\right]^{\frac{2}{5}}\left[(\bar{R}_n^2)^{\frac{2}{5}} + (\bar{R}_m^2)^{\frac{2}{5}}\right]\sum_{P\neq a}\left(\frac{R_\infty}{E_p}\right)^{4/5}V_p^{3/5}N_1^P \tag{12}$$

where α is a fine structure constant, V_p the perturber relative velocity, E_p the characteristic energy of the perturbing specie, and $\bar{R}_n$ and $\bar{R}_m$ the mean radial matrix elements. The relative velocity of perturbers can be calculated by

$$\mathrm{V}_p = \left[\frac{8kTN_0}{\pi}\left(\frac{W_a+W_p}{W_p \cdot W_a}\right)\right]^{\frac{1}{2}} \tag{13}$$

where W is the atomic weight with the subscript a and p representing species a or p. The mean radial matrix element $\bar{R}_X$ is expressed as [3]

$$\bar{R}_X{}^2 = \left(\frac{\mathrm{N}_X^{*2}}{2\mathrm{Z}_a^2}\right)[5\mathrm{N}_X^{*2} + 1 - 3\mathrm{l}_X(\mathrm{l}_X + 1)] \tag{14}$$

where Z_a is the net charge of specie a. X here can be m or n and l_X is the orbital angular momentum quantum number. N_X^* indicates the effective principal quantum number which is given as

$$\mathrm{N}_X^{*2} = \frac{\mathrm{Z}_a^2 E_H}{E_\infty^a - E_X^a} \tag{15}$$

where E_∞^a and E_X^a are, respectively, the ionisation energy and energy on level X of species a. Similarly, E_H is the ionization energy of a hydrogen atom.

2) Continuum radiation and absorption

Continuum radiation from a plasma is due to two mechanisms, free-bound electron recombination and free-free bremsstrahlung radiation. Under LTE condition, as the plasma is collision dominated in terms of energy exchange and transition of electronic states, Kirchhoff's law remains valid to relate spectral absorptivity to emission coefficient. Spectral absorptivity can be related to photon absorption cross section σ^a. The main problem in the calculation of continuum absorption is to obtain the cross section data. There is a lack of experimental results about photon absorption cross sections. Thus, in the present work some of the cross sections are estimated using theoretical methods.

Quantum Defect Method [25] and its variants are chosen to generate the photon absorption cross sections for atomic species. This method has been used by Liebermann and Lowke [4]. An LS coupling scheme is required first

$$\mathrm{E}_i^a(nlSL) = \sum g(J)E^a(nlSLJ)/g(nlSL) \tag{16}$$

where $g(J) = 2J + 1$ and $g(nlSL) = (2\mathrm{S} + 1)(2\mathrm{L} + 1)$. S and L are, respectively, the spin angular momentum and orbital angular momentum in LS coupling. Equation (16) defines the threshold energy for photon absorption. The frequency ν_{nl} of the energy level is then worked out. The cross section of photon absorption leading to ionisation is then expressed as

$$\sigma_{nlSL}^a = 8.559 \times 10^{-23}\left(\frac{\mathrm{E}_i^a(nlSL)+k^2}{\mathrm{E}_i^a(nlSL)^2}\right)\sum_{l'=l\pm1} C_{l'}|nl;Sl|^2 \tag{17}$$

where $k^2 = z_f^2 S$ is the energy of the ejected electron in Rydberg unit with z_f being the charge on the final ion. The unit of cross section from Equation (17) is in m^{-2}. According to the theory of free-bound transition, the frequency that the cross section in Equation (17) corresponds to is a threshold frequency. The cross section higher than the threshold frequency varies as $1/\nu^3$

$$\sigma_{\nu,i}^a = \sigma_{\nu_{th},i}^a(\nu_i/\nu)^3 \tag{18}$$

where $\sigma_{\nu_{th},i}^a$ is the cross section obtained from Equation (17). ν_i corresponds to the threshold frequency of the level with energy $\mathrm{E}_i^a(nlSL)$.

The photon absorption cross section for ions can be estimated using hydrogenic approximations. Combining with the estimation of frequency beyond the threshold, the following equation expresses the photon absorption cross section for ions

$$\sigma_{\nu,i}^a = \alpha a_0^2 4\pi^2 \frac{N_i^*}{Z_a^2}\left(\frac{\nu_i}{\nu}\right)^3 \tag{19}$$

where N_i^* is the effective principal quantum number of i^{th} energy state. Z_a is the net charge of the ion as seen by the valence electron. As the high energy levels tend to have small gaps, the absorption coefficient $\sum_i \sigma_{i,\nu}^a N_i^a$ can be treated as an integral. Thus the free-bound and all free-free radiation from all high energy levels is

$$\kappa_\nu^{bf+ff}(T,P) = \frac{kTa^3c^2}{4h\nu^3}\sum_a \frac{N_a}{U_a} Z_a^2 \eta_a \sum_K G_K exp\{-(E_\infty{}^{a,K} - \Delta E_\infty{}^a - h\nu')/kT\} \tag{20}$$

where η_a is a correction factor for species a which is set as two [24], G_K the statistical weight of the K^{th} parent term, $E_\infty{}^a$ the ionisation energy of species a, and $\Delta E_\infty{}^a$ the lowering of ionisation energy. ν' is defined as $\nu' = \nu_n = (E_\infty{}^{a,K} - E_n{}^{a,K})/h$ if $\nu \geq \nu_n$. For $\nu < \nu_n$, $\nu' = \nu$. $E_n{}^{a,K}$ is the lowest smeared energy state of species a.

For molecular continuum radiation, the calculation method is similar to atomic species. The cross sections of some of the species can be found from literature, such as C_2F_4 (i, neutral) [26], CF_4 (i, ii, iii) [27]-[29], C_2 (i) [30], F_2 (i) [31] and N_2 (i) [32]. The cross sections of the remaining species such as C_2N_2, CF_3, CF_3N, C_2F_2 and FN are estimated by two empirical methods which have been used successfully in [33]. The whole wavelength is divided into three regions separated by two boundary wavelengths. The first region is for all wavelengths shorter than a boundary wavelength (Table V). The photon absorption cross section is taken as a constant. The third region is for all wavelengths longer than the second boundary wavelength across which the photon absorption cross section is also assumed to be a constant. The middle region has a parabolic profile between the logarithm of the cross section and the wavelength, which is expressed by

$$\sigma_{r2} = 10^{a\lambda^2+b\lambda+c} \tag{21}$$

and is used to determine the boundaries for each species that do not have experimental photon absorption cross section. The coefficients are from [33]. According to the number of atoms contained in a molecule, the species can be divided into two groups. The first one is small molecules which include no more than three atoms, such as FN. The second group is formed by molecules with more than three atoms such as: C_2N_2, CF_3, CF_3N and C_2F_2. Following the method described in [33], the boundaries used in molecular cross section estimation are listed in Table V.

D. Net emission coefficient (NEC) and sources of fundamental data

The NEC is defined as the effective radiation emitted in a unit solid angle from a unit volume of gas located on the axis of an infinitely long and isothermal gas cylinder. It is defined as

$$\varepsilon_N(T,p,R_p) = \int_0^\infty \kappa_\nu(T,p) B_\nu(T) \exp\left(-\kappa(T,p)R_p\right) d\nu \quad (22)$$

where $\kappa_\nu(T,p)$ is the total spectral absorption coefficient including line and continuum absorption. $B_\nu(T)$ is the Planck function for blackbody. As it is stated before, Kirchhoff's law is applicable for LTE plasma at individual frequency level. The emission coefficient ε_ν is $\varepsilon_\nu = \kappa_\nu(T,p)B_\nu(T)$. Equation (22) considers the absorption of radiation in the isothermal cylinder when radiation travels from the centre of the plasma column out of the cylinder. To reduce the calculation time, the integration operation is discretised as

$$\varepsilon_N(T,p,R_p) = \sum_{\nu^K=\nu^{K-1}+d\nu} \kappa_\nu(T,p) B_\nu(T) \exp\left(-\kappa(T,p)R_p\right) d\nu \quad (23)$$

where ν^{K-1} is the frequency at position K-1 on the frequency axis and the next frequency point is equal to $\nu^{K-1} + d\nu$. Because of the narrow profile of line spectra, $d\nu$ has to be very small. A value of $10^{11} Hz$ is used in the NEC calculation.

Due to the large number of fundamental data that are needed in the calculation, it is not possible to list them all individually. Apart from the data source quoted in the tables, many of the atomic data come from a single source and therefore are deferred to this section. The energy level data of atoms that are used in the present work are gathered from the latest databases of the National Institute of Standards and Technology (NIST) [20]. Its Atomic Spectra Database (ASD) includes observed transitions and energy levels of most known chemical elements. The wavelengths of spectral lines included in ASD are from 0.002 nm to 60 nm. The data of spectral lines in ASD includes radiative transition probabilities and the energies of ground states and ionization. There are also other data sources such as those compiled by Kurucz (University of Hannover) [21] and by University of Harvard which include the spectral lines and atomic data for most common chemical elements. In our selection of data, experimentally obtained data with specified accuracy are the first choice. In the absence of any published data, estimation based on available theoretical model or empirical expressions are used. This will inevitably introduce uncertainties in the results. Therefore, it is necessary to compare some of the results for pure N_2 or pure PTFE with existing published work to characterise the method of calculation although a quantified error bar cannot be derived.

TABLE V
Boundary wavelength values used to separate the continuum radiative photo-absorption cross section of atoms into three regions [33].

Molecule	Boundary of Region 1-2(nm)	Boundary of Region 2-3(nm)
FN	115.3	135.3
C_2N_2	122	163.4
CF_3	135.2	165
CF_3N	138.9	173.7
C_2F_2	83.7	108.6

III. Representative Results of Equilibrium Composition and Net Emission Coefficient

A. Equilibrium composition

Two sets of equilibrium composition of nitrogen and PTFE mixture at atmospheric pressure are given in Figures 1 and 2. The percentage is in molar of nitrogen or PTFE at the temperature of 300 K. Due to recombination, CF_4, C_2N_2 and C_2F_3N are formed at around 800 K. However, the weak chemical bonds of these three species lead to their rapid dissociation above 4,000 K. Starting from 1,200 K, the number density of CF_3 rapidly increased. Dissociation of C_2F_4 starts at 3,000 K, which results in a large amount of carbon and fluorine atoms in the plasma. This is also the reason why the number density of CF_2, C_2F_2, CN rise in the temperature range from 2,800 K to 3,200 K. When the temperature is higher than 4,000 K, other remaining molecular species start to dissociation.

In practice radiation transfer in a flowing plasma burning in PTFE vapour and N_2 mixtures starts to become important when the temperature is above 10,000 K. It is clear that at this temperature the plasma composition in both mixtures is atom or electron dominated. One would naturally expect that the NEC of PTFE-N_2 mixtures above 10,000 K be similar to the NEC of the dominating atomic, ionic species and electrons.

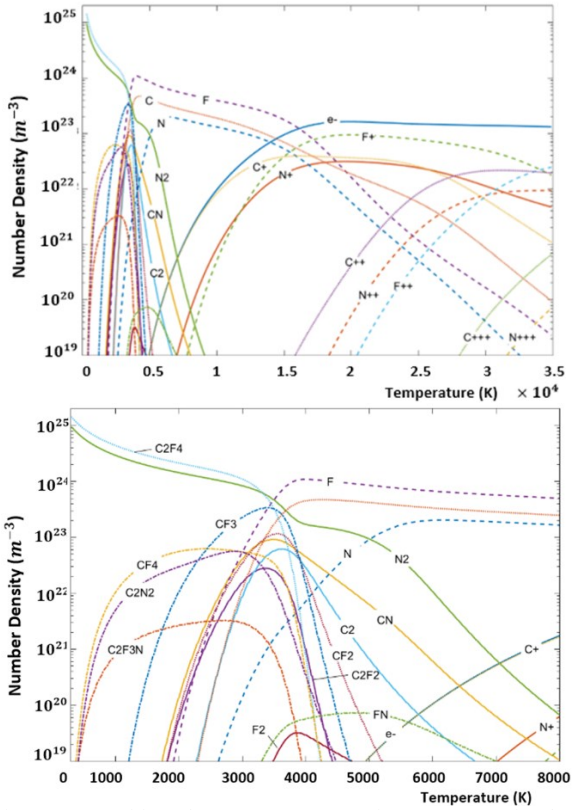

Fig. 1. Composition of 50%N_2-50%PTFE mixture. Pressure is 1 bar.

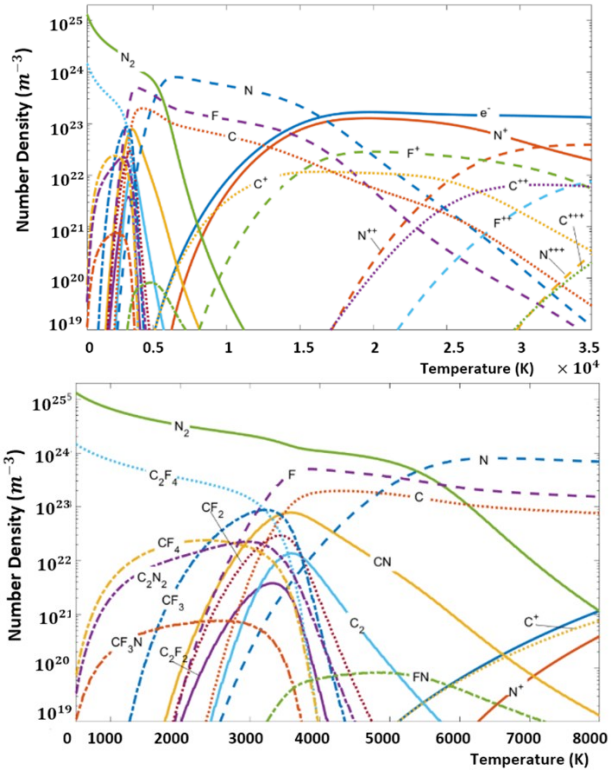

Fig. 2. Composition of 90%N_2-10%PTFE mixture. Pressure is 1 bar.

B. *Absorption coefficients*

The total number of atomic lines considered in the calculation is 32644. The frequency steps in the NEC calculation are optimised by trial in different regions to reduce the computation time to an acceptable level. The frequency of radiation is swept over a range from 0.1 Hz to 10 PHz. When the temperature increase to 5,000 K, most of the molecular species are dissociated. The number density of electrons dominates the composition when temperature is above 15,000 K. Since the temperature in the central core of switching arcs reaches typically 20,000 K, the calculated radiation absorption coefficients of 90%N_2-10%PTFE for temperatures 5,000 K,

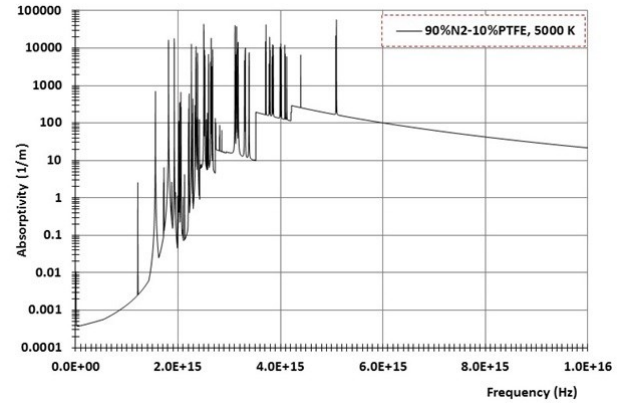

(a) 5000 K

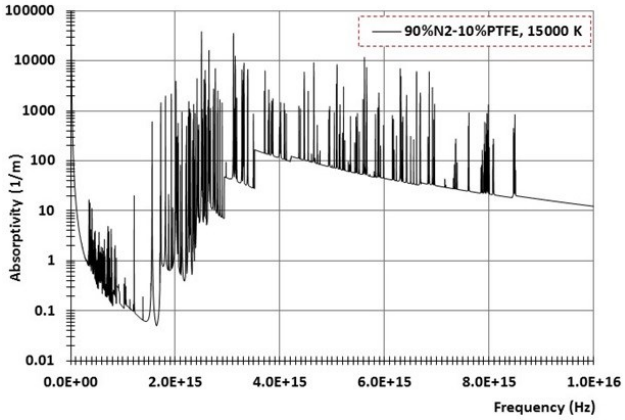

(b) 15,000 K

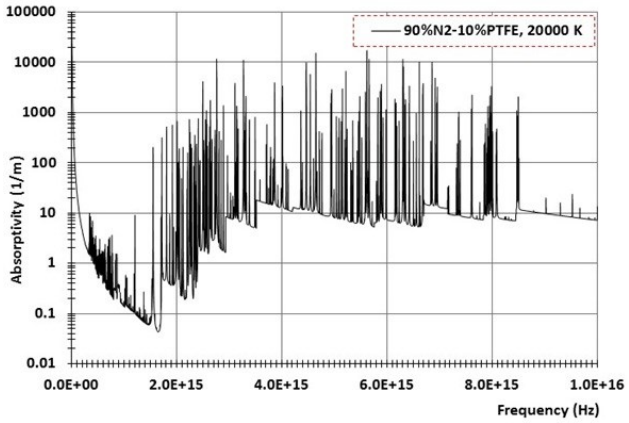

(c) 20,000 K

Fig. 3. Line and continuum absorption coefficient for 90% N_2-10% PTFE at temperature of (a) 5,000K; (b) 15,000K; and (c) 20,000K. Pressure is 1 bar.

15,000 K and 20,000 K with a pressure of 1 bar are presented in Figure 3. As expected the absorptivity of visible light (0.43 – 0.75×10^{15} Hz) at 5,000 K is negligibly small but there is strong absorption of higher frequency photons in the range from 1.5×10^{15} Hz to 4.5×10^{15} Hz. Figure 3(b) also shows the spectral resolution of the absorptivity curve as an inset. The resolution is sufficient to resolve the line profile. It is also clear that when the temperature increases, more high frequency lines (photons) are emitted, increasing the emitting power.

A comparison of the absorption coefficient at different pressures but with the same temperature is given in Figure 4. Denser plasma absorbs more radiation, both line and continuum. But there is more increased absorption of the continuum. The increase in absorptivity becomes less significant when the pressure goes from 10 bar to 100 bar. The absorptivity behaves in a similar way at the other temperatures.

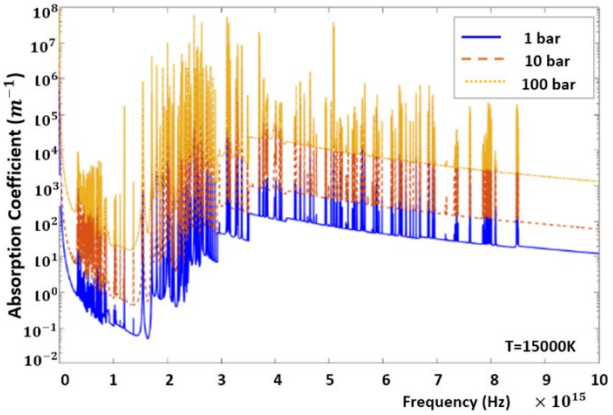

Fig. 4. Comparison of line and continuum absorption coefficient for 90% N_2-10% PTFE mixture with different pressures of 1 bar, 10 bar and 100 bar, at temperature of 15,000K.

C. *Net emission coefficient*

Figure 5 shows the NEC for 90% nitrogen–10% PTFE mixture with different emission radius for temperature higher than 8,000 K. Referring to the composition given in Figure 2, it is clear that the rapid increase in NEC corresponds to a temperature range of 10,000 K to 14,000 K where both electron and ion number density increases at a high rate and the electron number density soon becomes saturated with further increase in temperature from 14,000 K. Results show that the NEC of the gas mixture depends mainly on the atomic ion and electrons. Another feature of the NEC profiles is that with respect to temperature most of the radiation emitted from the centre is absorbed in the first millimeter. At 20,000 K nearly 90% is absorbed.

Strictly speaking, the definition of NEC is not applicable to most of the practical applications of thermal plasma because there is always spatial gradient of temperature, especially in the radial direction of the plasma column. Thus success in the use of NEC to approximately account for radiation loss from the plasma column relies on the choice or calculation of an equivalent radiation emission radius. More details will be given in Section 4.

Despite that the trend of change of NEC as a function of temperature is similar at different concentration of PTFE,

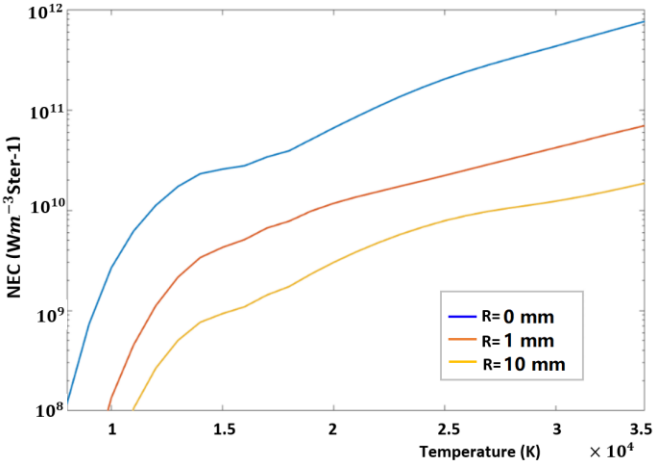

Fig. 5. The net emission coefficient of 90% N_2–10% PTFE plasma with different emission radius at a pressure of 1 bar.

nitrogen species emit more radiation than PTFE under identical conditions, which is shown in Figure 6. The plasma of 90% N_2 emits 4 time more radiation than the 10% gas mixture at 20,000 K. The NEC calculated by Chervy et al. [34] for CF_4 is shown in Figure 6 as filled circles. Since the mixture of 10% N_2 – 90% PTFE and CF4 both have atomic fluorine and atomic fluorine ion as the dominant positive species, their NEC are close to each other. The difference is caused by other ionic species.

Figure 7 presents the NEC for the mixture of 90% N_2 – 10% PTFE at different pressures (1 and 100 bar). Results at other mixing ratios are expected to behave similarly. It is shown that for optically thin plasma (R_{NEC} = 0), NEC is proportional to pressure. However with radiation absorption considered (R_{NEC} >0) there is no simple scaling laws. For example, with R_{NEC} = 1 mm at 20,000 K, the ratio corresponding to 100 bar and 1 bar is about 10 instead of 100.

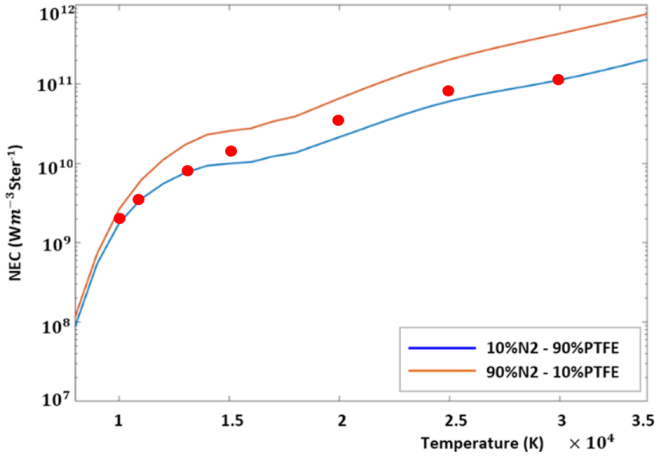

Fig. 6. Comparison of NEC with emission radius of 0 for 10% N_2 – 90% PTFE and 90% N_2 – 10% PTFE at a pressure of 1 bar. 10% N_2-90% PTFE is the top curve. Filled circles are the corresponding NEC of pure CF4 [34].

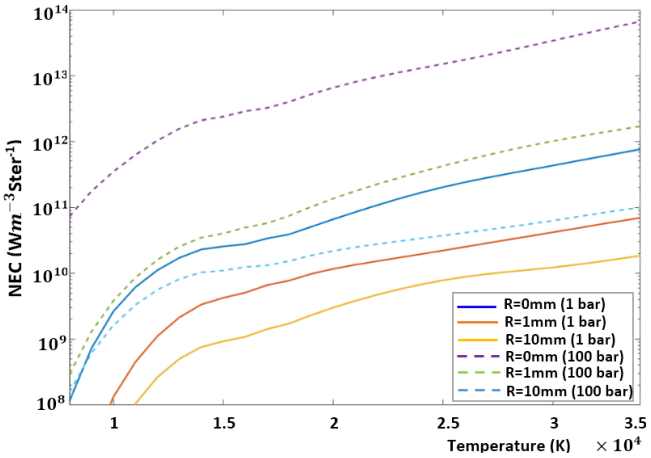

Fig. 7. Comparison of NEC for 90% N_2 – 10% PTFE mixture at pressures of 1 bar and 100 bar. For each group as shown in the legend, the curves move downwards when the pressure increases.

D. *Comparison with existing data and discussion*

The calculated NEC values (Figure 8) for pure nitrogen gas agree reasonably well (within 10%) with those calculated by Gleizes *et al.* [35] for temperatures above 13,000 K with an emission radius of 0 mm, i.e. no absorption is considered. The difference is in the temperature range from 8000 k to 13,000 K with the results given in [35] being higher than those from the present work by a factor of up to 2. Our results are slightly higher than those given by Allen [36]. There is a fair agreement with the results of Hermann and Schade [37]. The results of Ernst et al. [38] were obtained experimentally for a 1 mm radius arc. The values presented in Figure 8 are the radiation term (divergence of radiative energy flux) derived from energy balance and then divided by a solid angle of 4π. As will be discussed in Section 4, this value should be lower than the NEC. The scattering in the experiment can be as high as 16%. Given the differences in the atomic data used we argue that the calculated results are reasonable. Our calculated value is higher than the measured value over the temperature range of 12,000 K to 24,000 K.

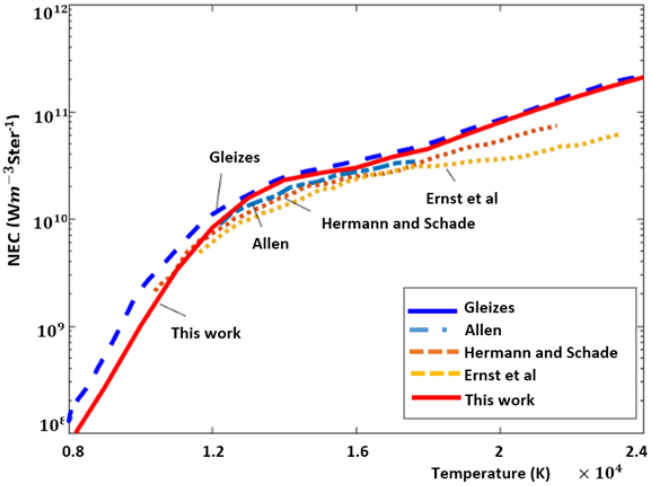

Fig. 8. Comparison of the calculated NEC of pure nitrogen gas at 1 bar with existing calculated and experimental results.

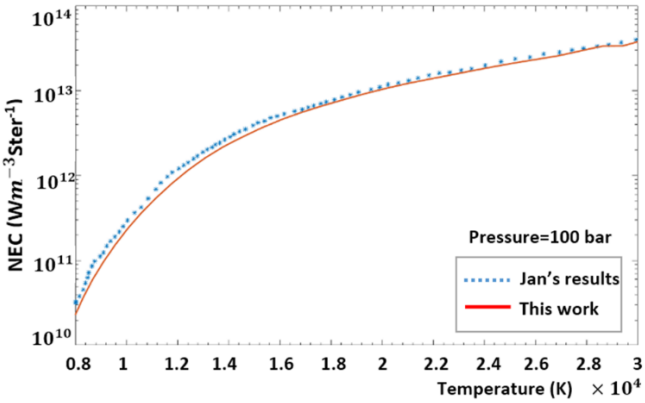

Fig. 9. Comparison of the NEC of pure PTFE vapour at 100 bar with that given in [33].

To further check the calculation method towards high PTFE concentration, an extreme case at 100 bar for pure PTFE is compared with that published by Jan *et al.* [33] for an emission radius of 0 mm. As shown in Figure 9, for the NEC lower than 16,000 K, the results given in [33] are slightly higher than the present results. The agreement becomes excellent for temperature above 16,000 K.

IV. Radiation Transfer in Nitrogen-PTFE Plasmas

Arc modelling requires the knowledge of the radiative source term in the energy equation. This term can be obtained using accurate method based on the radiation transfer equation (RTE) or using approximate methods, such as the semi-empirical model based on NEC [5], the partial characteristics method [7] or the P1 model [6]. It has been shown that the Discrete Ordinate Method (DOM) is able to give better accuracy in the calculation of the divergence of the radiative flux [13]. Over each chosen direction, the contribution towards the divergence can be derived from the radiation transfer equation for a single wavelength as

$$\nabla \mathrm{F}_v = \kappa_v \sum_j^n \omega_j \left[B_v(0) e^{-\int_0^{L_{wall,j}} \kappa_v(l_j) dl_j} - \int_0^{L_{wall,j}} \left(B_v(l_j) - B_v(0) \right) \kappa_v(l_j) e^{-\int_0^{l_j} \kappa_v(\zeta_j) d\zeta_j} dl_j \right] \quad (24)$$

where j designates a direction for integration which starts from a point on the integration domain boundary (Point S in Figure 10) and ends at the target point, i.e. the point of calculation (Point P in Figure 10). n is the number of directions over which integration of Equation (24) is performed. $L_{wall,j}$ is the length of the line segment from Point P to Point S. lj means the distance from any point on Line PS to Point P. $B_v(0)$ is the Planck function at l=0, i.e. at Point P. Equation (24) has also to be integrated over frequency to account for the contributions from all wavelengths. ω_j is a weighting factor associated with the finite number of integration directions uniformly distributed

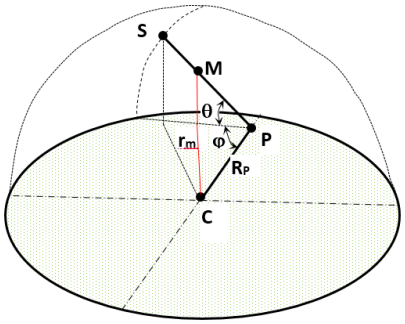

Fig. 10. Geometric relationship that is used to define the length of integration (PS) inside a spherical space. It is to be noted that this sphere is placed inside the arc column with C on the column axis and line CP perpendicular to the axis. The temperature only depends on the radius of the cylindrical column.

over the 4π angular space. Its value is equivalent to the solid angle that each direction covers

$$\omega_j = d\varphi * [\sin\left(\theta_j + \frac{1}{2}d\theta\right) - \sin(\theta_j - \frac{1}{2}d\theta)]d\varphi \; and \; d\theta \tag{25}$$

The radial distributions of the divergence of radiative energy flux for two typical temperature profiles are obtained with the DOM method. Two integration spaces have been used for the calculation. The first one is a cylindrical column with a length of 10 times its radius. The second space is a sphere, as shown in Figure 10. It must be noted that although a spherical space is used for evaluating the divergence of the radiative energy flux, the temperature is only a function of the column radius, i.e. r_m in Figure 10. The difference between these two cases is the length of line segment PS. For the same directional angles of θ and φ, line PS is longer in the cylindrical column case since S represents the intersecting point between a line in the given direction and the cylinder surface. The length of line PS for a spherical space is

$$L = R_P cos\theta cos\varphi + \sqrt{R_0^2 - R_P^2 + R_P^2 cos^2\theta cos^2\varphi} \tag{26}$$

where R_0 is the radius of the cylindrical column. For integration over the cylindrical column, the length of PS is

$$L = \frac{R_P cos\varphi + \sqrt{R_0^2 - R_P^2 sin^2\varphi}}{cos\theta} \tag{27}$$

which shows that when the integration direction becomes vertical (θ = π/2) the length of PS becomes infinite. Thus in the present work it is limited to 5 times the radius of the column (R_0). For any point M on PS, its corresponding radius that is used to obtain the local temperature is, for both cases,

$$r_M = \sqrt{R_P^2 + l_M^2 cos^2\theta - 2R_P l_M cos\theta cos\varphi} \tag{28}$$

where l_M is the distance from point P to point M on line PS.

Test calculations have shown that a frequency step size of 10^{12} Hz is appropriate in the integration. Further reduction does not lead to any significant improvement to the results. During the integration over a chosen direction, a maximum interval of 0.1 mm and a minimum interval of 0.05mm is used depending on the length of line PS. In the calculation, line PS is divided into 200 equal parts and an interval is calculated. This interval is then capped to be within the given range. Temperature profile 1 is constructed by [16]

$$T(r) = T_a - (T_a - \frac{T_0}{1-\exp(-5)})\left[1 - \exp(-5\left(\frac{r}{R_0}\right)^3)\right] \tag{29}$$

And temperature profile 2 is constructed by [13]

$$T(r) = T_0 + \frac{T_a - T_0}{2}\left[\mathrm{erf}\left(\frac{\beta + r}{\alpha}\right) + \mathrm{erf}(\frac{\beta - r}{\alpha})\right] \tag{30}$$

where T_0 is the temperature of the cold surrounding region and T_a the maximum temperature at the arc centre. α and β are two control parameters defining the profile of the distribution. R_0 is the radius of the gas column. Further information is given in Table VI for the two temperature profiles chosen in this study.

For the temperature profiles given in Figure 11, the temperature on the axis is 25,000 K and that at the radial boundary is 3,000 K. The radius of the gas column under consideration is 10 mm. The radial temperature distribution is discretised into 50 equal-distanced points in the calculation, which is sufficient to resolve the radiative flux and its divergence. It is to be noted that with the DOM method the divergence of the radiative flux is evaluated in three dimensional space despite the temperature distribution in the cylinder is only dependent on the radial coordinate of the column. Since the integration is only carried out in one quadrant

TABLE VI
Temperature profiles and their control parameters and radiation absorption percentage.

Features	For temperature profile 1	For temperature profile 2
Profile control parameters	T_0 = 3,000 k T_a = 25,000 K R_0 = 0.01 m	T_0 = 3,000 k T_a = 25,000 K α = 0.0005 β = 0.007
Arcing conditions in HVCB	Slender arc column, appearing normally in the period shortly before current zero where the current is moderate and the arc burns in high speed axial flow.	Fat arc column with a thin layer of relatively colder gas surrounding the arc column. This profile is representative during the high current phase of a self-blast circuit breaker where the arc is cooled by the injection of nozzle vapour due to ablation by strong arc radiation.
Scaling factor to fit DOM5-3 results to DOM15-12 results	0.74	0.72
Absorption layer thickness	3.6 mm	1 mm
Absorption density peak location	30% of total thickness from starting radial position.	30% of total thickness from starting radial position.
Percentage of radiation from arc core absorbed at edge	60%	36%

of the whole space, the true divergence should be the calculated value multiplied by a factor of 4. Unless indicated specifically, all results are obtained with a cylindrical column integration space whose length is 10 times the column radius.

Results in Figure 11 show that for an arc column with steep temperature gradient at its edge, the absorption density ($\nabla \cdot F$) is sensitive to the number of directions included in the integration. The use of fewer directions leads to an over-evaluation of the divergence. For the "top-hat" profile, the net emission from the centre of the plasma column is 2.93×10^{11} W/m^3 using DOM5-3 settings, which is 41% higher than that computed using DOM15-12 with a total number of 720 directions of integration. Increasing the number of integration improves the accuracy rapidly. Practically using DOM12-9 should produce reasonably accurate results for the divergence.

Using the spherical integration space only leads to a slightly higher divergence at the middle of the column and slightly lower absorption density peak at r = 7 mm in Figure 11 (the curve labelled as sphere domain). This indicates that regardless the huge variation in the absorptivity of the gas with frequency, hot gas that is 10 mm away from the calculation point P hardly contributes to the net radiative energy loss. It would be safe to use a spherical space for the evaluation of the divergence of the radiative flux.

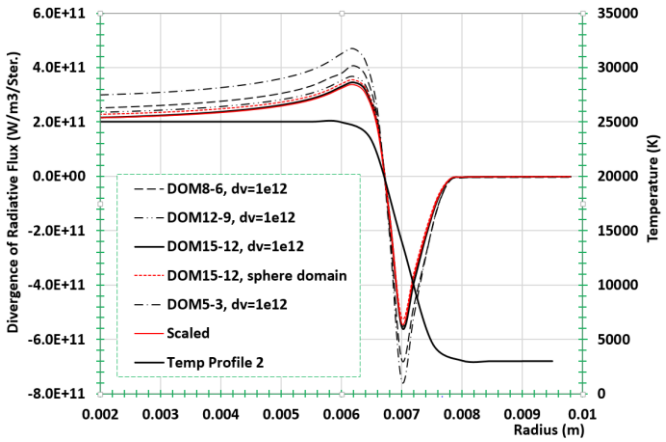

Fig. 11. Effect of the number of directions used for evaluating the divergence of the radiative flux using the DOM. Results are for 90N_2-10%PTFE at 1 bar with temperature profile 2. dv is frequency interval used in integration.

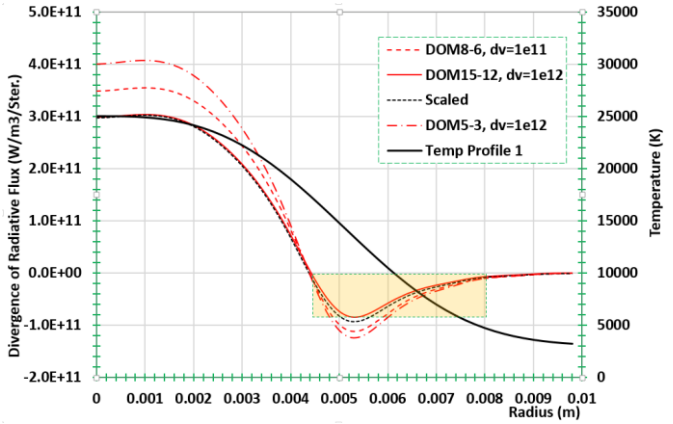

Fig. 12. Effect of the number of directions used for evaluating the divergence of the radiative flux using the DOM. Results are for 90N_2-10%PTFE at 1 bar with temperature profile 1. The rectangle indicates width of absorption layer.

Another important consideration is if it is possible to scale the results from DOM5-3 to obtain values close to the accurate results. As shown in Figure 11, the results from DOM5-3 are scaled using a factor that is the ratio of DOM15-12 to DOM5-3 at r = 0. It is surprising that the scaled values are basically identical to the accurate results. The same scheme is also applied to the temperature profile 1 with results given in Figure 12 where the scaled emission part of the curve is identical to the accurate results and the absorption part is only slightly higher than the accurate result. The scaling factor is 0.74 for temperature profile 1 and 0.72 for temperature profile 2. This scaling factor is in fact related to the weight of the chosen directions. For large intervals of θ and φ, the length of line PS varies substantially for different directions inside the angular element of dθdφ. In addition, the difference between the two scaling factors also depends on the temperature distribution near the surface of the column.

Radiation absorption at the arc edge becomes extremely important for arcs burning in self-blast high voltage circuit breakers. The determination of the location of the absorption layer is often challenging with simplified models. Results in Figures 11 and 12 show that the DOM method is able to accurately determine the boundary of the absorption layer and the location of the absorption density peak. For temperature profile 1 (Figure 12), net absorption starts at 4.5 mm and effectively ends at 8 mm. The absorption peak occurs at 5.4 mm. For temperature profile 2, absorption starts at 6.8 mm and ends at 8 mm with the absorption peak occurring at 7 mm. For both cases, the absorption density reaches its maximum in the negative direction at a point whose distance to the starting point of the absorption layer is 30% of the total thickness of the absorption layer. For temperature profile 1 (slim arc), 60% of radiation from the arc core is absorbed. For temperature profile 2, only 36% of the radiation from the arc core is absorbed despite the stronger absorption density shown in Figure 11.

Theoretically, the NEC calculated from Equation (23) for an isothermal hot gas cylinder is not equal to the divergence of the radiative energy flux evaluated over the 4π angular space. The NEC has not considered the radiation absorbed by the emitting particles which is sent out by gas from other locations in the cylinder. Therefore $4\pi\varepsilon_N$ should be larger than $\nabla \cdot F$. Results given in Figure 13 supports the argument.

Temperature profile 2 is closer to an isothermal arc column since the gas temperature remains at 25,000 K up to the point of r = 6 mm. The temperature then drops rapidly to 3,000 K when r = 8 mm. We can define two emission radii, one corresponding to 83% of the axis temperature and is equal to 6.5 mm and the other one is equal to 8 mm, corresponding to the point when the temperature drops to 3,000 K. The NEC

values corresponding to these two radii are shown in Figure 13 as shaded rectangles, both being higher than the $\nabla \cdot F$ term calculated in the present work.

For temperature profile 1, it is difficult to define an equivalent emission radius. Using a radius of 3.8 mm, which corresponds to 83% of the axis temperature, leads to a value of $4\pi\varepsilon_N$ that is 40% higher than the accurate value. Using the average value of $R_{83\%}$ and R_{5000K} for temperature profile 1 [39], we have an effective radius of 5.9 mm. The corresponding NEC based on the local temperatures are shown by the filled circles in Figure 13. It can be seen that when the equivalent emission radius is chosen reasonably, the NEC can be a good approximation of the divergence of the radiative energy flux.

The width of the absorption layer used in a simplified 1D model [39] was also shown for the two temperature profiles in Figure 13 by the slightly shaded dotted rectangles. The width is equal to $R_{83\%}$ - R_{5000K}. The layer width for temperature profile 1, as marked by the rectangle below the zero divergence line is larger than that obtained by the DOM. For temperature profile 2 the absorption layer thickness is only slightly smaller, as depicted by the rectangle above the zero divergence line. This implies that the simplified model defines the absorption layer width more accurately for the high current phase of high voltage gas-blast circuit breakers because the radial temperature distribution moves towards a "top-hat" profile at high current.

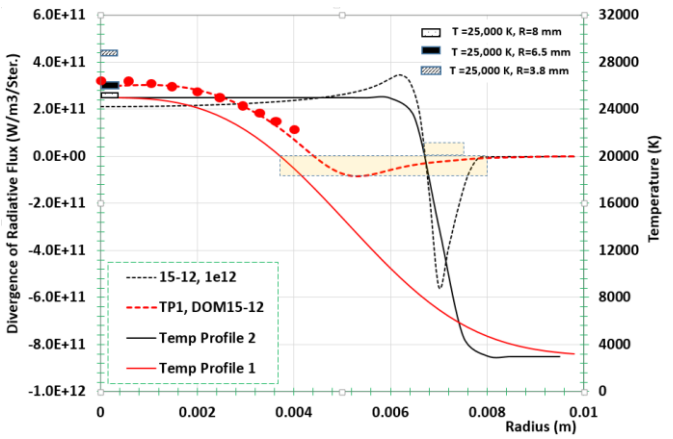

Fig. 13 Divergence of the radiative energy flux for two typical radial temperature profiles encountered in high voltage circuit breakers and comparison with the NEC calculated using different definitions of the emission radius. Rectangles with dotted sides indicate the absorption layer thickness according to the method in [39].

V. Conclusions

The net emission coefficient (NEC) of nitrogen plasma contaminated by PTFE vapour is calculated in the present work based on fundamental theory. The radiation transfer characteristics of the N_2-PTFE vapour mixture is then studied using the Discrete Ordinate Method (DOM). The validity of the NEC calculation method is assessed by comparing the NEC values for pure N_2 and pure PTFE with published data, showing that the method used in the present work has a reasonable level of accuracy.

Our study shows that for radial temperature distributions typically encountered in high voltage gas-blast circuit breakers the DOM12-9 configuration is able to calculate the divergence of the radiative energy flux with very good accuracy (difference less than 5%). Although the DOM5-3 configuration over-estimates the divergence, it can accurately define the location and size of the absorption layer (only one absorption layer in the present work). For the two very different radial temperature profiles used, the maximum absorption density is located at a point whose distance to the starting radial position is 30% of the total thickness of the absorption layer. There is a possibility to scale the results from DOM5-3 to recover the accurate results using a scaling factor between 0.7 – 0.8. The validity of this approach has however to be tested with more radial temperature profiles.

Although very useful information is obtained towards the development of a more accurate simplified 1D model for radiation transfer calculation for switching arcs, there are still important issues that need to be addressed. The first one would be the pressure variation inside the arc column, which requires a three-dimensional interpolation of the absorptivity locally (frequency, temperature and pressure). Secondly, more typical temperature profiles encountered in high voltage circuit breakers, including temperature variation in the axial direction, need to be used to test the findings reported in the present work.

The actual PTFE concentration in a circuit breaker is not uniformly distributed and it also changes with time since the arcing process is transient. For calculation of radiation transfer, we will need to use the absorption coefficient based on the local value of the concentration in the integration process.

References

[1] H. Knobloch, "The comparison of arc-extinguishing capability of sulfur hexafluoride (SF_6) with alternative gases in high-voltage circuit-breakers," in Gaseous Dielectrics VIII, New York: Plenum, pp. 565-571, 1998.

[2] H. R. Griem, "Semiempirical formulas for the electron-impact widths and shifts of isolated ion lines in plasmas," Phys. Rev., vol. 165, p. 258, Jan. 1968.

[3] J. Cooper, "Plasma spectroscopy," Rep. Progr. Phys., vol.29, no. 1, p.35, 1961.

[4] J. Lowke and R. Liebermann, "Predicted arc properties in sulfur hexafluoride," J. Appl. Phys., vol. 42, no. 9, pp. 3532-3539, 1971.

[5] J. L. Zhang, J. D. Yan, A. B. Murphy, W. Hall, and M. T. Fang, "Computational investigation of arc behavior in an auto-expansion circuit breaker contaminated by ablated nozzle vapor," IEEE Trans. Plasma Sci., vol. 30, no. 2, pp. 706-719, Apr. 2002.

[6] D. Godin, J. Trepanier, M. Reggio, X. Zhang, and R. Camarero, "Modelling and simulation of nozzle ablation in high-voltage circuit-breakers," J. Phys. D: Appl. Phys., vol. 33, no. 20, p. 2583, 2000.

[7] G. Speckhofer, R. Gilles, W. Smith, and M. Bures, "A consistent set of thermodynamic properties and transport coefficients for high temperature plasmas," in Proc. 14th Int. Symp. On Plasma Chem., pp. 269-274, 1999.

[8] J. Jeans, "Stars, gaseous, radiative transfer of energy," Monthly Notices of the Roy. Astronomical Soc., vol. 78, pp. 28-36, Nov. 1917.
[9] V. Kourganoff, "Basic Methods in Transfer Problems," Oxford: Clarendon Press, 1952.
[10] M. F. Modest, "Radiative heat transfer," Academic press, 2013.
[11] V. G. Sevast'yanenko, "Radiative transport in the real spectrum. Integration over frequency," J. Eng, Phys, vol. 36, Issue 2, pp. 138-148, 1979.
[12] M. R. Charest, C. P. Groth, and Ö. L. Gülder, "Solution of the equation of radiative transfer using a Newton–Krylov approach and adaptive mesh refinement," J. Comput. Phys., vol. 231, pp. 3023-3040, 2012.
[13] A. Iordanidis and C. Franck, "Self-consistent radiation-based simulation of electric arcs: II. Application to gas circuit breakers," J. Phys. D: Appl. Phys., vol. 41, no. 13, p. 135206, 2008.
[14] M. Seeger, L. Niemeyer, T. Christen, M. Schwinne, and R. Dommerque, "An integral arc model for ablation controlled arcs based on CFD simulations," J. Phys. D: Appl. Phys., vol. 39, no. 10, p. 2180, 2006.
[15] J. J. LOWKE, "Predictions of arc temperature profiles using approximate emission coefficients for radiation losses," J. Quant. Spectrosc. Radiat. Transf., vol. 14, no. 2, pp. 111-122, 1974.
[16] P. Kloc, V. Aubrecht, M. Bartlova, and O. Coufal, "Radiation transfer in air and air-Cu plasmas for two temperature profiles," J. Phys. D: Appl. Phys., vol. 48, no. 5, p. 055208, 2015.
[17] P. Scarpa, B. Dauby, J.M. Defise, W. Legros, M. Barrault, G. Bernard, and S. Rowe, "SF_6 auto-expansion circuit breaker design: numerical and experimental investigations of arc-gas interactions," IEEE Trans. Power Del., vol. 7, no. 1, pp. 339-45, Jan. 1992.
[18] J.D. Yan and M.T.C. Fang, "The effects of self-induced magnetic field on a high current SF_6 arc in a supersonic nozzle", in Proc. 23rd Int. Conf. Phenomena Ionised Gases, vol. 2, Toulouse, France, pp. 148-149, 1997.
[19] D. Godin and J. Trépanier, "A robust and efficient method for the computation of equilibrium composition in gaseous mixtures," Plasma Chem. Plasma process., vol. 24, no. 3, pp. 447-473, 2004.
[20] NIST Atomic Spectra Database Levels. Available: http://physics.nist.gov/PhysRefData/ASD/levels_form.html, [Accessed: 12th-Feb-2015].
[21] Atomic Spectral Line Database from CD-ROM 23 of R. L. Kurucz. Available: http://www.pmp.uni-hannover.de/cgi-bin/ssi/test/kurucz/sekur.html, [Accessed: 12th-Feb-2015].
[22] M. Chase and C. Davies Jr, "NIST-JANAF Thermochemical Tables", 4th ed. New York, NY, USA: American Institute of Physics for the National Institute of Standards and Technology, 1998.
[23] W. L. Wiese, M. W. Smith, and B. Glennon, "Atomic Transition Probabilities. Volume 1. Hydrogen through Neon," DTIC, Fort Belvoir, VA, USA, Tech. Rep. NSRDS-NBS 4, 1966.
[24] R. Liebermann and J. Lowke, "Radiation emission coefficients for sulfur hexafluoride arc plasmas," J. Quant. Spectrosc. Radiat. Transf., vol. 16, no. 3, pp. 253-264, 1976.
[25] A. Burgess and M. Seaton, "Radiative recombination of He," Monthly Notices of the Roy. Astronomical Soc., vol. 121, p. 471, August 1960.
[26] S. Eden, P. Limao-Vieira, P. Kendall, N. Mason, J. Delwiche, M.-J. Hubin-Franskin, et al., "Electronic excitation of tetrafluoroethylene, C_2F_4," Chem. Phys., vol. 297, no. 1, pp. 257-269, 2004.
[27] L. G. Christophorou, J. K. Olthoff, and M. Rao, "Electron interactions with CF4," J. Phys. Chem. Reference Data, vol. 25, no. 5, pp. 1341-1388, 1996.
[28] L. Lee, E. Phillips, and D. Judge, "Photoabsorption cross sections of CH_4, CF_4, CF_3Cl, SF_6, and C_2F_6 from 175 to 770 Å," J. Chem. Phys., vol. 67, no. 3, pp. 1237-1246, 1977.
[29] J. W. Au, G. R. Burton, and C. Brion, "Quantitative spectroscopic studies of the valence-shell electronic excitation of freons ($CFCl_3$, CF_2Cl_2, CF_3Cl, and CF_4) in the VUV and soft X-ray regions," Chem. Phys., vol. 221, pp. 151-168, Aug. 1997.
[30] N. Padial, L. Collins, and B. Schneider, "Photoionization of ground-state molecular carbon C_2," Astrophys. J., vol. 298, pp. 369-374, Nov. 1985.
[31] A. Orel, T. Rescigno, B. McKoy, and P. Langhoff, "Photoexcitation and ionization in molecular fluorine: Stieltjes − Tchebycheff calculations in the static - exchange approximation," J. Chem. Phys., vol. 72, no. 2, pp. 1265-1275, 1980
[32] Y. Itikawa, "Cross sections for electron collisions with nitrogen molecules," J. Phys. Chem. Reference data, vol. 35, no. 1, pp. 31-53, 2006.
[33] C. Jan, Y. Cressault, A. Gleizes, and K. Bousoltane, "Calculation of radiative properties of SF_6–C_2F_4 thermal plasmas—application to radiative transfer in high-voltage circuit breakers modelling," J. Phys. D: Appl. Phys., vol. 47, no. 1, p. 015204, 2013.
[34] B. Chervy, H. Riad, and A. Gleizes, "Calculation of the interruption capability of SF_6-CF_4 and SF_6-C_2F_6 mixtures. I. Plasma properties," IEEE Trans. Plasma Sci., vol. 24, no. 1, pp. 198-209, Mar. 1996.
[35] A. Gleizes, B. Rahmani, J. Gonzalez, and B. Liani, "Calculation of net emission coefficient in N_2, SF_6 and SF_6-N_2 arc plasmas," J. Phys. D: Appl. Phys., vol. 24, no. 8, p. 1300, 1991.
[36] R. A. Allen, "Air radiation tables," NASA Tech. Rep., CR-557, 1967.
[37] W. Hermann and E. Schade, "Radiative energy balance in cylindrical nitrogen arcs," J. Quant. Spectrosc. Radiat. Transf., vol. 12, no. 9, pp. 1257-1282, 1972.
[38] K. Ernst, J. Kopainsky, and H. Maecker, "The Energy Transport, Including Emission and Absorption, in N_2-Arcs of Different Radii," IEEE Trans. Plasma Sci., vol. 1, no. 4, pp. 3-16, Dec. 1973.
[39] Y. Pei, J. Zhong, J. Zhang, and J. Yan, "A comparative study of arc behaviour in an auto-expansion circuit breaker with different arc durations," J. Phys. D: Appl. Phys., vol. 47, no. 33, p. 335201, 2014.

Jianying Zhong Received the BSc degree from Xi'an Jiaotong University in 1997 and obtained the MSc and PhD degrees from Shenyang University of Technology in 2002 and 2006, respectively. Since then she has been working in Pinggao Group Co. Ltd. Her research focuses on switching arcs and HV, EHV, HVDC, UHV and UHVDC equipment.

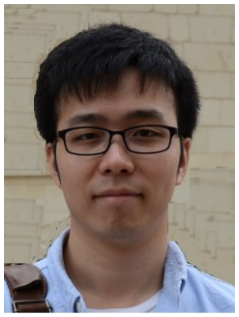

Fei Yang received the BEng degree in 2011 and PhD degree in 2016 from the University of Liverpool. His research interest is in the field of calculation of thermodynamic properties, transport coefficient and radiation characteristics of high pressure plasmas under both equilibrium and non-equilibrium conditions.

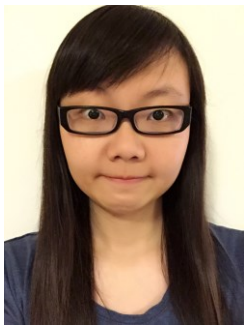

Wen Wang received the BSc degree in 2011 from the PLA Information Engineering University (China), and the MSc degree in 2012 from the University of Birmingham. She is currently a PhD student in the University of Liverpool with research interest in the field of contact erosion and nozzle ablation in intelligent high voltage circuit breakers.

Duanlei Yuan received the MSc degree from Zhengzhou Institute of Light Industry in 2006. Since 2006, he has been a Research Engineer with Pinggao Group Co. Ltd., Pingdingshan City, Henan Province, China. He is currently a Senior Engineer with the Technology Centre of the Group, also located in Pingdingshan City. His current research interest includes intelligent electrical apparatus, especially switchgear.

Joseph (Jiu Dun) Yan received the BEng and MEng degrees from Tsinghua University (Beijing) in 1986 and 1988, respectively, and obtained the PhD degree at the University of Liverpool in 1998. He has since been with the University of Liverpool and is currently Professor in Applied Electromagnetism. His research interests include switching arcs, plasma physics, SF_6 replacement, and more recently electrical discharges in HVDC insulation.